

PCCP

Accepted Manuscript



This is an *Accepted Manuscript*, which has been through the Royal Society of Chemistry peer review process and has been accepted for publication.

Accepted Manuscripts are published online shortly after acceptance, before technical editing, formatting and proof reading. Using this free service, authors can make their results available to the community, in citable form, before we publish the edited article. We will replace this *Accepted Manuscript* with the edited and formatted *Advance Article* as soon as it is available.

You can find more information about *Accepted Manuscripts* in the [Information for Authors](#).

Please note that technical editing may introduce minor changes to the text and/or graphics, which may alter content. The journal's standard [Terms & Conditions](#) and the [Ethical guidelines](#) still apply. In no event shall the Royal Society of Chemistry be held responsible for any errors or omissions in this *Accepted Manuscript* or any consequences arising from the use of any information it contains.

Capacitance Spectroscopy and Density Functional Theory

Paulo R. Bueno^{1}, Gustavo T. Feliciano, Jason J. Davis*

¹Institute of Chemistry, Physical Chemistry Department, Univ. Estadual Paulista (São Paulo State University, UNESP), Nanobionics group (www.nanobionics.pro.br), CP 355, 14800-900, Araraquara, São Paulo, Brazil.

²Department of Chemistry, University of Oxford, South Parks Road, Oxford OX1 3QZ, UK.

ABSTRACT

The redox capacitance and its associated quantum component arising from the charging of molecular levels from coupled metallic states is resolvable and quantified experimentally by capacitance spectroscopy (CS). Herein we both relate this N -electron system capacitance directly to conceptual chemistry density function theory (DFT) and the charging magnitude and associated quantum capacitive term (which resemble those introduced by Serge Luryi¹), to the Kohn-Sham frontier molecular orbital associated energies for isolated molecules and DFT calculated redox Density of States (DOS) for metal-molecule junctions for single molecule and molecular films confined at metallic interfaces. DFT computational analyses reveal the orbital energetic alignment between iron redox site and those states in the metal specifically when metal-molecule junction are formed. The impact of this on the resolved chemical softness and capacitance is also revealed. These analyses, additionally, are shown to numerically resolve redox capacitance in a manner which accurately reproduces experimental observations for molecular films. These observations both theoretically underpin CS and provide guidance as to its optimised application in interfacial analyses involving molecular electrochemistry and derived sensory applications.

KEYWORDS: Quantum capacitance, molecular electronics, molecular electrochemistry, capacitance spectroscopy, electroactive molecular films, Density Function Theory.

Corresponding author

Phone: +55 16 3301 9642; Fax: +55 16 3322 2308

Email: [*prbueno@iq.unesp.br](mailto:prbueno@iq.unesp.br)

1. INTRODUCTION

Capacitance Spectroscopy

Capacitance spectroscopy (CS)² is a methodology based on the resolved ratio between a time-dependent current response and an imposed small amplitude voltage applied to molecular scale films. We have previously shown that this enables a quantification of an electron chemical (redox) capacitance and its associated quantum components within energetically addressable molecular films,^{2,3} and that these charging characteristics, in the past loosely ascribed to “pseudo capacitance” (or faradaic capacitance),⁴ represent a specific manifestation of the general mesoscopic capacitance^{5,6} principles introduced by Marcus Buttiker.⁷ This electron chemical capacitance, is redox (faradaic) capacitance (C_r) where energetic donor/acceptor states are associated with reduced and oxidized chemical states in the molecular film, arises specifically from the coupling of a supporting electrode density of states [$g_m(E)$] to the redox sites molecular density of states [$g_r(E)$].^{2,3,5,6} We note that this resembles concepts introduced by Serge Luryi¹ is his consideration of quantum capacitance in devices comprising an interphase boundary between a metal and a two-dimensional electron gas i.e., non a redox/electroactive configuration^{5,6} in which quantum capacitance was not theoretically associated with any electron chemical potential variation. It is also resolved free of non-faradaic capacitive components, i.e. those not associated with redox state occupancy.^{5,6} We have shown that C_r is comprised of two distinct series contributions thus $1/C_r = 1/C_e + 1/C_q$ (see Figure 3a), where C_e is the electrostatic or geometrical capacitance arising from charge separation in the normal (classical) sense and C_q the quantum capacitance, arising very specifically from the chemical potential changes associated when charging a nanoscale (atomic/molecular scale) entity.^{5,6}

In contrast with molecular electronic (conductance) measurements, where, in general, molecules of interest must bridge between two biased electrodes, CS constitutes a frequency-dependent single probe measurement.^{2,5,6} In this approach, since the electronic density of states in the metal is much higher than that associated with the addressable redox states of the molecule, it follows that variations in voltage impact the latter to a much greater extent such that $C_r \propto e^2 g_r(E)$. Statistically, for a distribution of redox states thermally

equilibrated with an electron bath, i.e. a redox active molecular film over metallic electrode, at room temperature, $g_r(E)$ is experimentally reported as a Gaussian redox density of states^{2, 3, 5, 6}; this DOS is exactly that of accessible redox states able to resonate with electrode states. In previous work we have shown that the environmental sensitivity of this DOS fingerprint (and associated redox charging accessed through redox capacitance analyses) can be usefully applied within diagnostic and biosensing applications.⁸⁻¹⁰

Conceptual Density Functional Theory

Density functional theory (DFT) is a powerful and appealing method for predicting the microscopic properties of matter. Quantum mechanically we start from the relevant Schrödinger equation for the system of interest, be it an atom, a molecule, or a solid, and resolve the observables of interest from the system's wavefunction. Though conceptually straightforward this is demanding for multi-electron systems and computationally prohibitive for large (e.g. biomolecular) systems. Because of this, density functional theory has, in the last decades, successfully replaced wavefunction approaches and has supported the computational study of large atomic/molecular systems where the ground-state particle density is obtained, in principle, containing all the information needed to know about the studied system, as demonstrated by Hohenberg and Kohn in 1964.¹¹

DFT has, now, a well-established potential for quantifying chemical characteristics and providing them with a theoretical basis.^{4, 12-18} This is the so-called conceptual DFT (also known as chemical or chemical reactivity DFT)^{4, 12-18} that was developed from the 1980's onwards and inspired by Robert Parr and coworkers.^{16, 18} It constitutes a basis on which to define a whole family of functions of the chemical/electronic response of an electronic system such as hardness and softness (as will be shown in detailed below), within the specific context of chemical (mesoscopic) capacitance. In DFT, the fundamental variable associated with all observables is, of course, the electron density, i.e. $\rho = \sum_i \psi_i^2$, where ψ_i can be expressed as a linear combination of Kohn-Sham orbitals. Numerous empirical atomic or molecular characteristics have evolved to enable predictions or explanations of chemical behaviour/reactivity.^{4, 13} One such parameter is electronegativity, χ , defined by Mulliken as the average of ionization potential I and electron affinity energies A , $\chi = 1/2(I + A)$.¹⁸ The

associated electron (or electronic) chemical potential, μ , is herein considered to be constant and defined (in DFT) as¹⁸

$$\mu = \left(\frac{\delta E}{\delta N}\right)_v = \left(\frac{\delta E}{\delta \rho}\right)_v = -\chi \quad (1)$$

where E is the electronic energy, N is the number of electron particles in a given N -electron system and μ is then clearly identified as the negative of Mulliken electronegativity. Thermal energy is disregarded here such that nuclei are considered to present a constant electrostatic potential. Finally, note that ρ is N per unit of volume (the electron density) and the third part of Eqn. (1) refers to the functional relationship between E and the electron density, ρ . Note also that both v and ρ are functions of \vec{r} (coordinate space) but, for simplicity, this is omitted herein (see SI. document for more detail). The theoretical (in conceptual DFT) definition of chemical hardness, η , has been shown¹⁸ to be $\eta = (\delta^2 E / \delta \rho^2)_v = (\delta \mu / \delta N)_v = (\delta \mu / \delta \rho)_v$, i.e. the derivative of the chemical potential with the number of electronic particles in the chemical system. The inverse of this function is

$$\sigma = \left(\frac{\delta \rho^2}{\delta^2 E}\right)_v = \left(\frac{\delta N}{\delta \mu}\right)_v = \left(\frac{\delta \rho}{\delta \mu}\right)_v \quad (2)$$

equivalent to the softness of the system. The basic idea behind the use of DFT that leads to the definition of Eqn. (2) and its inverse function (chemical hardness) or indeed other functions related to electron density, is that, in every reaction of an atom, molecule or chemical system (i.e. an given N -electron system) when perturbed through electron number or external potential, a measureable and proportional response is detected. We emphasise that the approach to be demonstrated herein is actually an example of the use of these reactivity descriptors in conceptual DFT in the specific case of redox reactions comprising molecular films. In so doing we seek to provide a DFT description of redox (faradaic) capacitance within molecular electrochemistry.

Now it is important to state that, in considering the mathematical methodology associated with Kohn-Sham formulation of finite-temperature density function theory,¹⁹ the energy defining equations arise as¹⁸

$$H_{KS}\psi_i(\vec{r}) = \varepsilon_i\psi_i(\vec{r}) \quad (3)$$

where H_{KS} is the Kohn-Sham Hamiltonian, $\psi_i(\vec{r})$ are the normalized Kohn-Sham orbitals and ε_i is the eigenvalue of that state. Eqn. (3) is related to the electron density by¹⁸

$$\rho(\vec{r}) = \sum_i |\psi_i(\vec{r})|^2 f(\varepsilon_i - \mu) \quad (4)$$

where $f(\varepsilon_i - \mu)$ is the Fermi-Dirac function $f(\varepsilon_i - \mu) = \{1 + \exp[(\varepsilon_i - \mu)/k_B T]\}^{-1}$. k_B is the Boltzmann constant and T the temperature. More details on H_{KS} and its relationship with μ are given in the SI. section 2. Changes in chemical potential between N -electron systems involve electron transfer (electrochemistry) such that (Figure 1), as predicted by the Gibbs free energy of electron chemical reactions, the associated energetics are quantified/rationalised by ionization and affinity energies within DFT.²⁰⁻²³

In this paper we focus on the charging processes inherently existing in molecular redox states tethered to metallic probes introduced above and discuss how this connects with mesoscopic physics, the electrochemistry of quantised states. Specifically we demonstrate the use of a conceptual DFT approach and CS to resolve classical and quantized energetic contributions within molecular electrochemistry and provide a rationalization of the resolved DOS and capacitance in terms of the softness of the molecular or nanoscopic system. We start by defining the capacitance of an N -electron system.

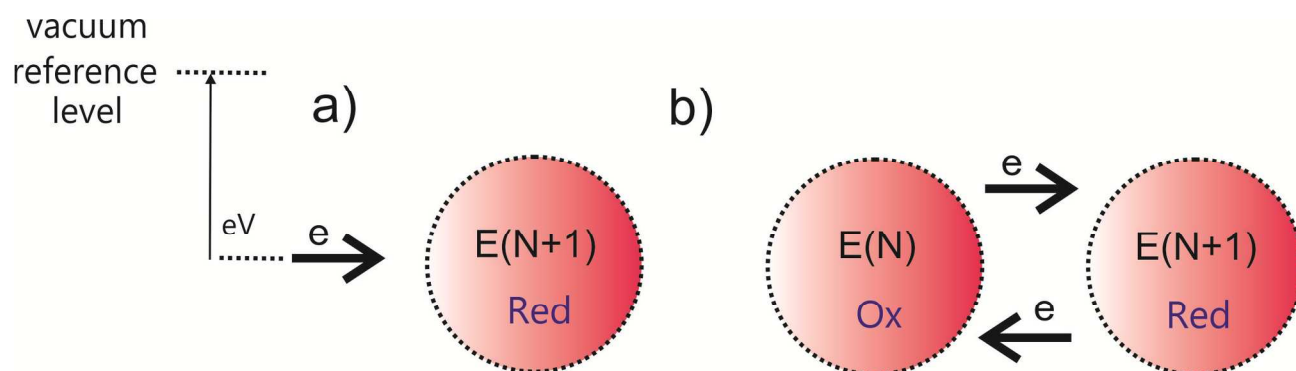


Figure 1. Schematic depiction of electron transfer or energy storage processes in either quantum or classical physical systems. (a) An electron being introduced to an N -electron system (atomic or molecular) from vacuum. The magnitude of associated energy change is the well-known electron affinity $[A(N)]$ or ionization potential $[I(N)]$ as discussed in the text. (b) An analogous representation of electron transfer between oxidized and reduced states of the same N -electron system. The (b) situation is particularly important in modelling the influence of redox entity electronic structure on electrode-confined electrochemical reactions (the focus of the DFT herein).

2. ELECTRONIC CHEMICAL POTENTIAL AND QUANTUM CAPACITANCE

The capacitance of an N -electron system

The capacitance that specifies the work, in terms of the electrical potential V , required to bring a fixed amount of charge dq from the vacuum level (see Figure 1a) to a particular chemical environment is defined as

$$\frac{1}{C} \equiv \frac{dV}{dq} \quad (5)$$

where $dq = e dN$, e is the unit of charge and N is the number of electrons in the chemical system at a given cartesian coordinate, \vec{r} , within the volume of the chemical system.

In contrast to the electronic energy associated with charging macroscopic electrodes (as depicted in Figure 2a), an equivalent process at atomic or molecular scales (Figure 1 and 2b), brings with it a concomitant change in the potential and thus chemical potential [Eqn. (1)] by

$$e dV = \mu(N + dN) - \mu(N) \equiv d\mu \quad (6)$$

In combining Eqn. (5) and (6) we are able to define $C_\mu = edq/d\mu$ as the capacitance associated with electron charging of a given N -electron system with respect to vacuum energy level (Figure 1a), the charging energy (with $dN = 1$) for a single electron transfer (in molecular scale) is

$$\frac{e^2}{C_\mu(N)} = \mu(N + 1) - \mu(N) \quad (7)$$

Note that Eqn. (7) represents twice of the work needed to move one electron from a vacuum dielectric reference under a fixed potential, i.e. twice the electrostatic energy stored on typical geometrical capacitors, C_e , i.e. $e^2/2C_e$. In practice, the relative contributions of C_μ and C_e are dependent on the sensitivity of chemical potential on orbital occupancy, something that is scale dependent. In considering now the total energy, $E(N)$, of an N -electron system then^{24, 25}

$$\mu(N) = E(N) - E(N - 1) \quad (8)$$

from which it can be observed that

$$I(N) = E(N - 1) - E(N) \quad (9)$$

and

$$A(N) = E(N) - E(N + 1) \quad (10)$$

where $I(N)$ and $A(N)$ are the ionization and association energies for the N -electron system. Since the finite-difference method²⁶ states that Eqn. (7) represents the difference between the ionization potential and electron affinity energies, we have^{19,20}

$$\frac{e^2}{C_\mu(N)} = E(N - 1) - 2E(N) + E(N + 1) = I(N) - A(N) \quad (11)$$

And now in dividing by 2 to establish an exact comparison with the electrostatic (geometry-predicted and stored) energy ($e^2/2C_e$) we arrive at exactly the definition of chemical hardness through capacitive analysis¹⁸ $\eta = e^2/2C_\mu(N) = [I(N) - A(N)]/2 = 1/2(\delta\mu/\delta\rho)_v$ from which it can be readily observed that the softness

$$\sigma = \frac{2C_\mu(N)}{e^2} = 2 \left(\frac{\delta\rho}{\delta\mu} \right)_v \quad (12)$$

is directly proportional to the DOS, i.e. $g_r(E)$ for the situation described in Figure 2b and 3b.

In summary, $C_\mu(N)$ is known as the electron chemical capacitance (redox capacitance if associated with redox charging)⁷ of an N -electron system, with an associated chemical energy [Eqn. (11)] experimentally accessible by CS and fundamentally connected to electronegativity, ionisation and chemical softness (or its inverse, hardness). In the next section we build upon these concepts within the context of DFT and specifically show that experimentally resolvable perturbation in $C_\mu(N)$ enables access through Eqns. (6), (7) and (12), to the chemical potential $d\mu$, hardness and softness. The former is responsive to underlying surface potential or local electrostatic change as, for example, induced by local chemical/biochemical recognition event, with a sensitivity that depends directly on the latter.⁸⁻¹⁰

3. CAPACITANCE SPECTROSCOPY AND DENSITY FUNCTIONAL THEORY

The capacitance of redox addressable molecular states^{2, 3, 5, 6}

The specific C_r (redox capacitance) charging fingerprint of an experimental configuration typified by Figure 2b contains both electrostatic (C_e) and chemical/quantum (C_q) contribution⁵ as noted above and this (see Figure 3a) is

$$\frac{1}{C_r} = \frac{1}{C_e} + \frac{1}{C_q} = \frac{1}{C_e} + \frac{1}{e^2 dN} \left[\left(\frac{\delta E}{\delta N_R} \right)_v + \left(\frac{\delta E}{\delta N_M} \right)_v \right] \quad (13)$$

In establishing an analogy to Eqn. (1), $\mu = (\delta E / \delta N_M)_v$ represents the electron chemical potential of electrons in the metallic phase and $1/g_r(E) = (\delta E / \delta N_R)_v$ that associated with redox states in molecular adlayer. As the density of states in the probe is massively higher than that of molecular layers, i.e. $g_m(E) = (\delta N_M / \delta E)_v \gg g_r(E) = (\delta N_R / \delta E)_v$, Eq. (13) turns into⁵

$$\frac{1}{C_r(N)} \equiv \frac{1}{C_e} + \frac{1}{e^2 g_r(E)} \equiv \frac{1}{C_e} + \frac{1}{e^2} \left(\frac{\delta E}{\delta N_R} \right)_v \quad (14)$$

In now considering exclusively the electrostatic energy (U_e) needed to move one electron from an electron reservoir state (for instance a given metallic electrode) to that associated with an orbital molecular state as given by $U_e = e^2 / 2C_e$ (the classic Coulomb blockade Coulombic term²⁷), Eqn. (14) can be then rewritten as

$$\frac{e^2}{C_r(N)} = 2U_e + \frac{e^2}{C_q(N)} \quad (15)$$

From this it can be noted that the relative dominance of the classical or quantum terms of the experimentally measured redox capacitance depends on a number of boundary conditions such as those associated with scale and geometry and on the relative magnitude of $g_r(E)$ with respect to C_e (the smallest term ultimately dominates C_r magnitude). In specifically considering a contact between an N -electron system with energy, $E(N)$, as depicted in Figure 3b, and a metallic plate electrode where the potential energy can be experimentally modulated, the electron distribution is tuned by charge transfer between the electrode and the molecule. The electrostatic component can be estimated by considering Gauss's law of the electromagnetism giving $C_e = \varepsilon \varepsilon_0 A / L$ (for a metal plate capacitor as depicted in Figure 2a or molecule-metal plate as in Figure 2b) where ε is the dielectric constant of the environment, ε_0 is the dielectric constant of vacuum and A and L are respectively, the area of the contact electrode and L is the distance between the electrode and the molecule.

Note that this term depends only on the geometry of the experimental system - this is why electrostatic (classical) capacitance is commonly referred to as the geometric capacitance. For typical experimental values associated with a molecular scale redox active film $A \gg L$ and, in additionally considering a distance of 1 nm between the redox and metallic states, then $C_e > 10^{-19}$ F, i.e. large such that C_q is expected to dominate the differential capacitance in CS experiments (those associated with scheme of Figure 2b).

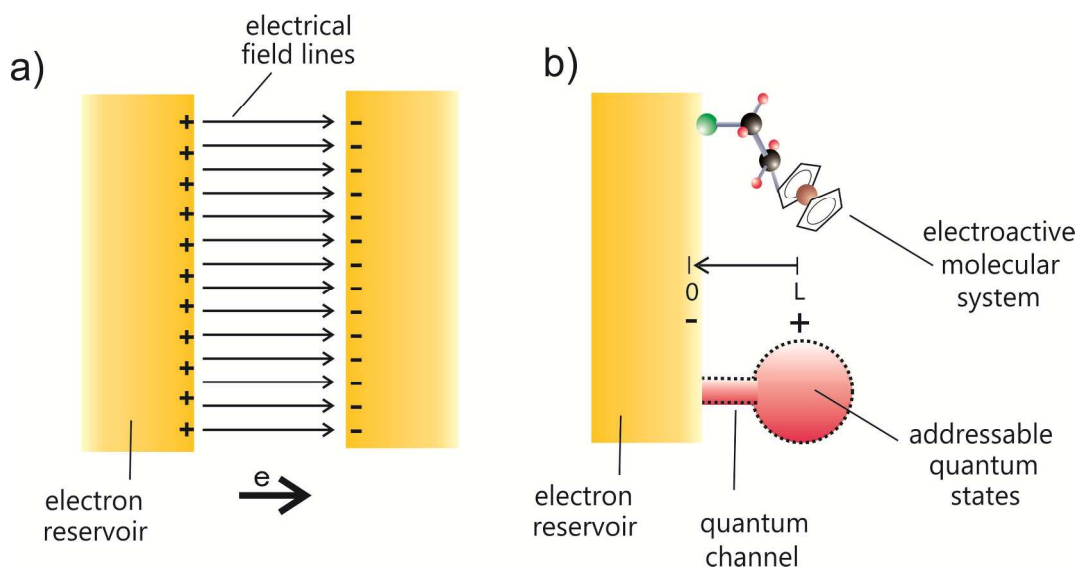


Figure 2. (a) The electron transfer involved in charging a parallel plate capacitor geometry (in this case the quantum characteristic is null). The arrows show the direction of electron flux. (b) A depiction of the charging of a molecular film or single molecule from a metallic density of states (electrode or an electron reservoir). Note the equivalence of a surface confined redox addressable state to a “quantum cavity” with its associated “quantum capacitance”.

Therefore, we arrive at an association of this electron chemical capacitive energy with the chemical properties of the system by following Eqn. (1) and (9),

$$I(N) = \chi(N) + \frac{e^2}{2C_q(N)} \quad (16)$$

and/or by following Eqn. (1) and (10)

$$A(N) = \chi(N) - \frac{e^2}{2C_q(N)} \quad (17)$$

where $\chi(N)$ is Mulliken electronegativity energy of the N -electron system (the molecular adlayer, Figure 2b).

The differences between Eqns. (16) and (17) leads to $e^2/C_q(N)$ in a manner analogous to Eqn. (11). Note that if

$\Delta U_e \ll e^2/\Delta C_q$ the redox energy variation [$e^2/\Delta C_r$] (in molecular redox layer) is governed by the chemical (quantum) term,^{5, 6} i.e. we have a situation in which the variation of the quantum component dominates any change in C_r . In the next section we give a meaning to the $e^2/C_q(N)$ for isolated molecular systems within the context of DFT and further we extrapolate this to molecular metallic junctions (including electrode-molecular films). The implication of the obtained results and conclusions has impact not only on our understanding of the influence of local environmental change on interfacial charging characteristic (as those schematically shown in Figure 2b) but also the application of this capacitive configurations within derived sensors.⁸⁻¹⁰

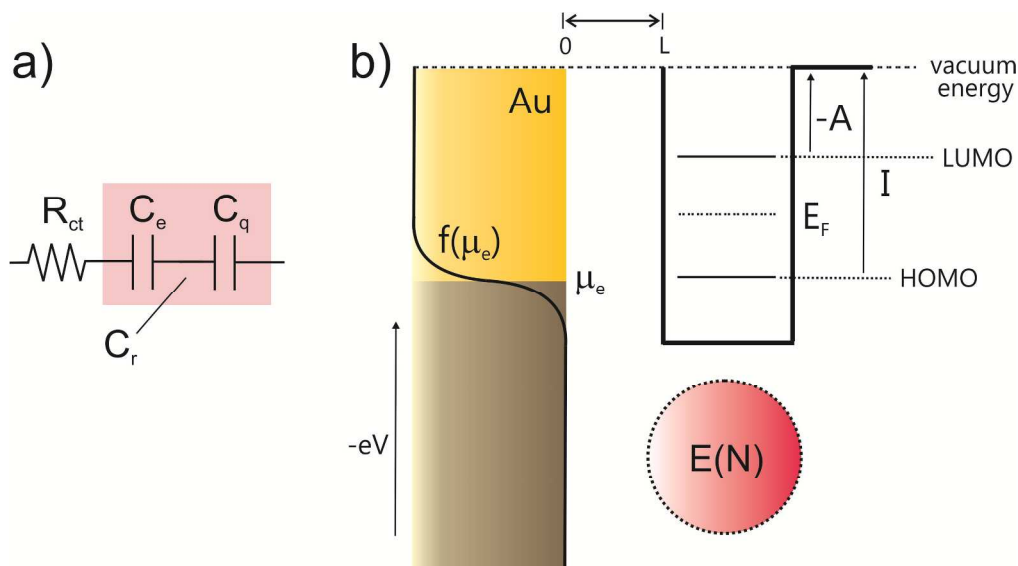


Figure 3. (a) The equivalent circuit depiction of redox activity at an electroactive molecular film modified metallic electrode, comprising charge transfer resistance, R_{ct} , and redox capacitance, C_r , the latter being divisible into electrostatic C_e and localized DOS (or quantum) based contributions, C_q . (b) An energy level model of a metallic plate electrode in contact with a quantum dot comprising a molecular structure [representing an N -electron system with an energy of $E(N)$]. The molecular structure is approximated by a square well with molecular energy levels defined relative to vacuum. The frontier orbital energies are shown - correspondence with DFT is stated through the difference between HOMO and LUMO energy levels [$\varepsilon_{N+1} - \varepsilon_N$, according to Eqn. (18)] and through the sum of $I(N)$ and $A(N)$ energies according to Eqn. (11). The spatial separation between addressable molecular states and those of the metal is given by L . E_F is the Fermi energy in the molecule, μ_e is the electron chemical potential of the electrons in the electrode, statistically governed by Fermi Dirac statistics, $f(\mu_e)$.

Kohn-Sham eigenvalues and quantum capacitance

In this treatment thus far there has been no consideration of the effects of thermal energy, i.e. DFT energies are reported under the framework of the zero temperature approximation. Thermal broadening is introduced later into DFT calculations if required. The importance of Eqn. (11), within this, is that a correlation can be made with Kohn-Sham eigenvalues as derived by DFT^{24, 25} (see SI. section 3 and the schematic illustration of Figure 3b),

$$\frac{e^2}{C_r(N)} = E(N-1) - 2E(N) + E(N+1) = \varepsilon_{N+1} - \varepsilon_N + 2U_e \quad (18)$$

where ε_{N+1} and ε_N are the lowest unoccupied (LUMO) and the highest occupied (HOMO) Kohn-Sham (KS) orbital energies and U_e is approximately a constant. It should be noted here (see SI. 3, particularly Eqn. SI. 27) that $e^2/C_q(N) = \varepsilon_{N+1} - \varepsilon_N$ for an isolated N -electron system (e.g. a spatially isolated molecular structure), a term that is directly proportional to the hardness [inversely proportional to the softness, according to Eqn (12)] of the chemical redox site.

The implications inherent within Eqn. (18) are electrochemically significant; the quantum term of the redox capacitance is implicitly given by the difference between ε_{N+1} (corresponding to the LUMO energy state of a redox active molecule) and ε_N (corresponding to the HOMO energy state of a redox active molecule) energies. Consequently, the capacitance of the redox molecular film is shaped by the electronic structure (described by Kohn-Sham orbitals in DFT) of the molecules coupled to metallic electrodes. The electronic wave function (calculated from DFT method) describing this redox active metal-molecule interface mathematically can lead to a continuum function [Eqn. (18) equates to (14) in this case] known as density of states (DOS) and then $C_q(N)$ is directly proportional to the DOS formed by redox states tethered to the electrode.

In the next section we demonstrate a test of Eqns. (14) and (18) within a DFT framework (both for isolated and electrode coupled molecules) and observe the qualitative impact of electronic structure on capacitance. We also quantitatively compare the computational results with CS resolved experimental values for molecular films.

4. CS EXPERIMENTAL RESOLUTION AND DFT COMPUTATIONAL RESULTS

In seeking a theoretical basis for the capacitance of an electroactive molecular film confined to a metallic electrode we represent this system with an atomistic model (see Figure 4) comprising a gold cluster in which ferrocene-hexanethiol (representing a well characterised and commonly used redox probe) is covalently attached and compare the calculated quantum properties of this to an analogous isolated ferrocenyl-hexanethiol (the protonated form of the thiol). The latter has 40 atoms and, is coupled to a gold metal slab of 300 atoms (see more details in SI. section 1.3). It is important to note that CS is only experimentally resolved for

the surface tethered film configuration since only here can the redox process store energy and an associated capacitance be measured by CS.²⁸

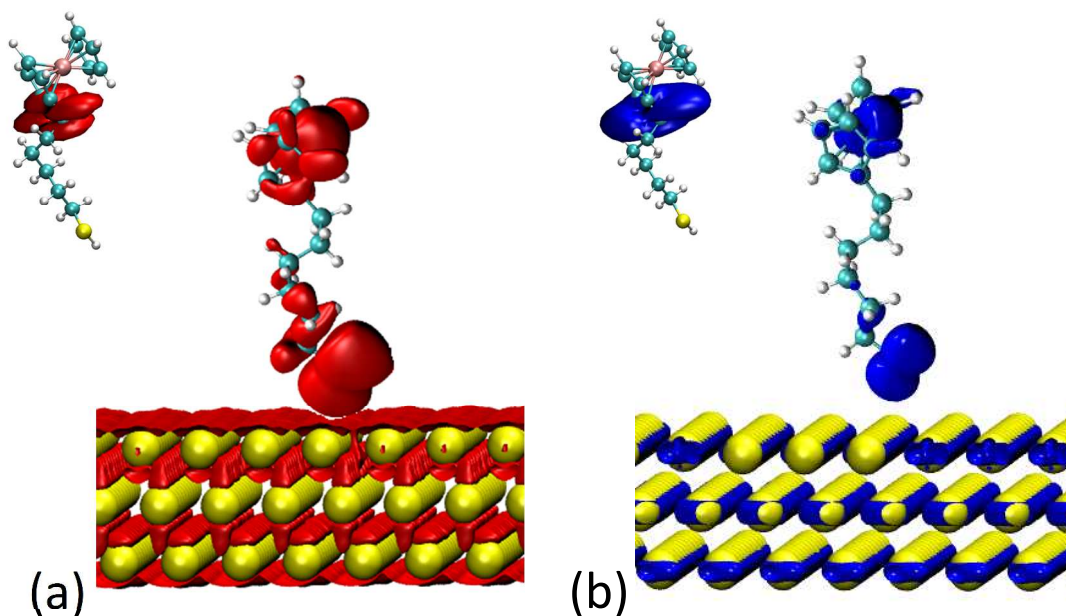


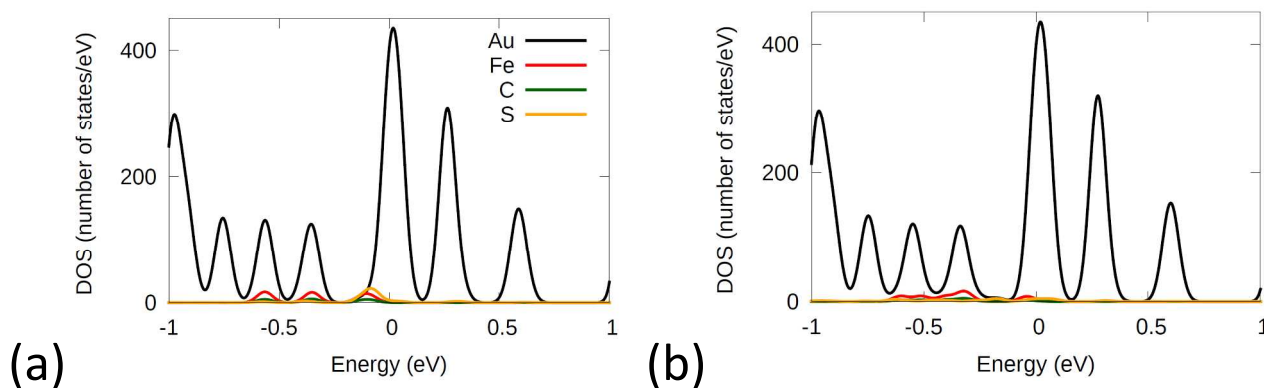
Figure 4. As discussed in the main text the positively charged gold cluster-alkylthiolate-ferrocenium $[\text{AuS}-(\text{CH}_2)_6\text{-Fc}^+]$ is the chemical entity that contributes most to the redox capacitance associated with this junction. DFT geometries and respective calculated isodensities are shown for both the LUMO state (red) and the HOMO (blue). Analogous depictions are shown for the isolated molecules in inset. The energy state alignment within the surface tethered configuration is notable.

In modelling both isolated and tethered molecular configurations (Figure 4) we can directly observe the influence of electronic structure arising from the electrode-molecule coupling on the capacitance through the generation of new energetic states and the contribution of this process to measurable charging. We additionally demonstrate that experimentally resolved quantum capacitance aligns well with DFT generated predictions of contributing orbital states (through Eqn. 18 and when it equates to 14), energetic alignment and decreased HOMO-LUMO separation.

We initially analyse, through Eqn. (14) and/or Eqn. (18), on the variation of the total energy of the system with respect to charge variation/electron occupancy. To avoid unnecessary computational complexity all DFT calculations were considered under vacuum conditions and zero absolute temperature [in order to access the intrinsic properties (so that quantized characteristic of the gold slab is observed in Figure 5) of the molecular system without having to sample over a range of thermally accessible conformations]. Once an initial ground

state is defined (by optimizing geometry according to DFT code, see SI. Section 1.4), the variation in chemical potential of the system with respect to electron exchange is accessible. The chemical potential of the system was evaluated by DFT across three states of charge in aligning with Eqn. (18), i.e. (a) the energy of the oxidized state, bearing N electrons, $E(N)$, the Fe(III) state here; (b) the energy of the reduced state, containing $N + 1$ electrons, $E(N + 1)$, the Fe(II) state here; and (c) the energy of $N - 1$ electron system, $E(N - 1)$. All energies were calculated (see Table 1) within the same molecular geometry for both isolated and tethered molecular systems, geometries (as shown in Figure 4) assumed to be invariant through electron exchange (computational technical details are described in SI. section 1.3 and 1.4).

Here it is worth noting again (Figures 4 and 5) that it is the ferrocenium entity that most prominently contributes to C_q charging because it is here where the HOMO and LUMO are mostly energetically aligned with underlying gold states. As shown, there is no evidence for iron and gold state energetic alignment for the neutral species, confirming the lack of neutral redox state contribution to the HOMO and LUMO electronic structure that modulates the redox capacitance.



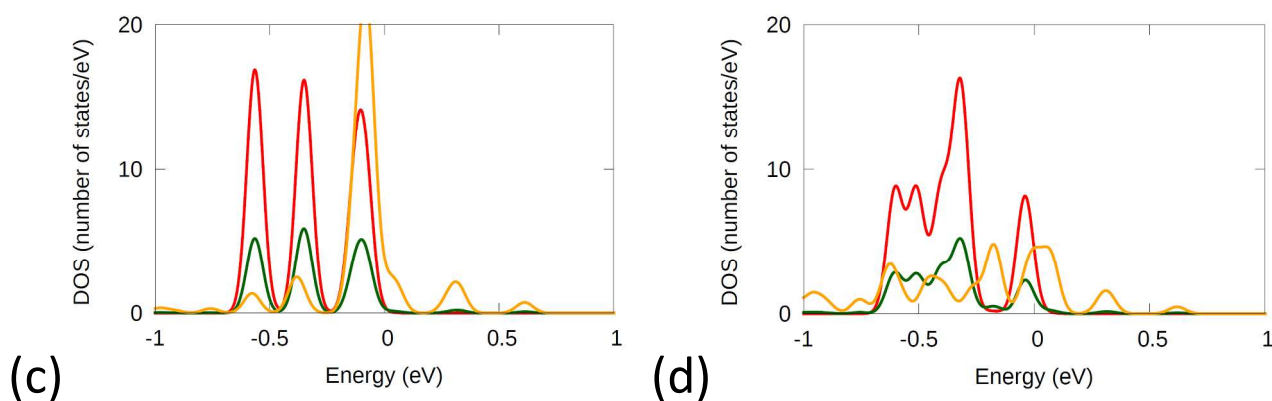


Figure 5. Projected DOS for (a) the $[\text{AuS}-(\text{CH}_2)_6\text{-Fc}]$ system and (b) $[\text{AuS}-(\text{CH}_2)_6\text{-Fc}^+]$ system and, the corresponding magnified views (c) and (d), showing the contribution of each atom to each projected molecular orbital. The relevant peaks are those closest to the zeroed Fermi energy level which serves as reference level between occupied and unoccupied states. The occupied states correspond to the peaks on the right (positive) with the unoccupied left (and negative). The DOS is obtained from a convolution product between the KS eigenvalue spectrum and a broadening Lorentzian function of width 0.05 eV that are not strong enough to eliminate the observed quantized behavior.

In Figure 6a the electronic structure of the isolated (positively charged) molecular system (geometry as shown in Figure 4) is shown together with the change associated with coupling to the metal slab (Figure 6b). Most significantly, we resolve here sufficient energetic alignment between the HOMO and LUMO states such that the system can be described as having an effective DOS function, an effect further pronounced if the thermal broadening effects (as shown Figure 6b, continuous line) are integrated through a consideration of Lorentz-Boltzmann statistics. This increased chemical softness in turn increases the associated quantum capacitance (according to Eqn. (12)). It is important to note that significant contribution to the energetic alignment and coupling of gold orbitals with iron orbitals is enhanced by 3d orbital of the iron itself and the carbon ring 2p states of the ferrocene (as evidenced by Figure 4 when comparing the molecule-metal system with the isolated molecule shown in the inset).

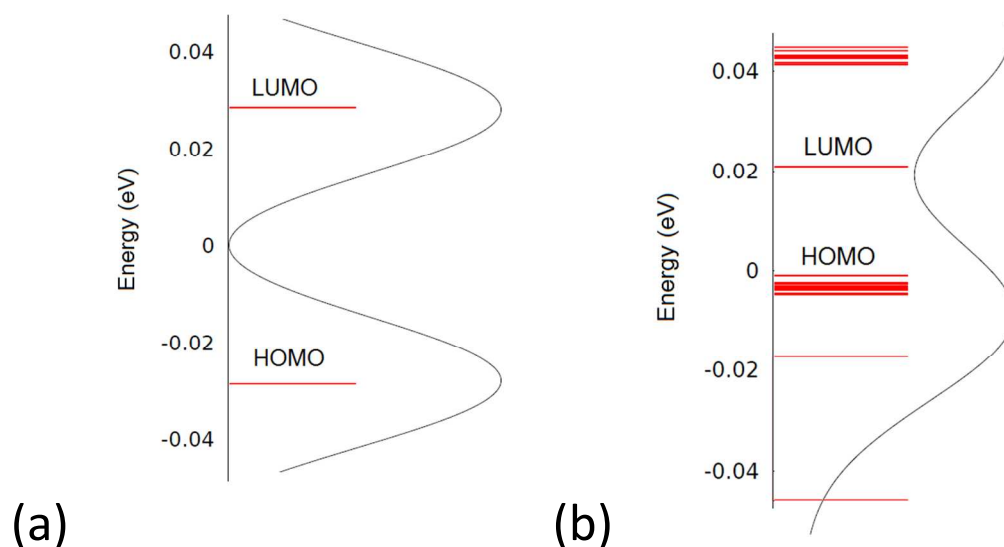


Figure 6. Kohn-Sham eigenvalue spectra (red lines), i.e. the energy states according to orbital analysis around the Fermi energy level for (a) isolated ferrocene-hexanethiol and (b) for ferrocene-hexanethiol tethered to a metal slab. In (b) the perturbation of orbital states by the presence of metallic states is evident. The additional states introduced in the metallic-molecular system between HOMO and LUMO and are additionally thermally broadened ($k_B T$, black smooth line, with T at room temperature, i.e. 298 K) and then describable by a continuum DOS function. The decreased HOMO-LUMO energetic gap and increased chemical softness directly impacts redox capacitance as discussed in the main text.

Using the energies obtained in Table 1 the quantum capacitance $e^2/C_q(N)$ contribution to the total capacitance was calculated by considering its correspondence with the differences between ε_{N+1} (LUMO eigenvalue) and ε_N (HOMO eigenvalue) of the molecular system following Eqn. (18). The resolved quantum capacitance (Table 1) also has, of course contributions which differ between the isolated and surface tethered configurations, in a manner which depends largely on the occupancy of 3d-states associated with the ferrocene center. The surface tethered system is softer by virtue of the new orbital states generated (gold derived states) and has an increased quantum capacitance compared to the isolated system.

Table 1. DFT calculated energies for the N -electron system considered herein, for both free [(HS-(CH₂)₆-Fc)] and surface confined [AuS-(CH₂)₆-Fc] configurations. These energies were subsequently utilised, though Eqn. (18) to calculate the redox capacitance (C_r). The Kohn-Sham orbital eigenvalues are noted as ε_{N+1} and ε_N . Note that $E(N)$ corresponds to the total energy and ε_N to the energy of the specific eigenvalue. Finally, C_r is the calculated in atto (a) faradays where a is equivalent to 10^{-18} (see SI. for more technical details).

	$E(N + 1)$ (eV)	$E(N)$ (eV)	$E(N - 1)$ (eV)	ε_{N+1} (eV)	ε_N (eV)	$C_r(N)$ (aF)
HS-(CH ₂) ₆ -Fc	-3900.462	-3895.099	-3886.345	-6.712	-6.773	0.047184
AuS-(CH ₂) ₆ -Fc	-273235.642	-273232.095	-273227.833	-3.899	-3.911	0.223776

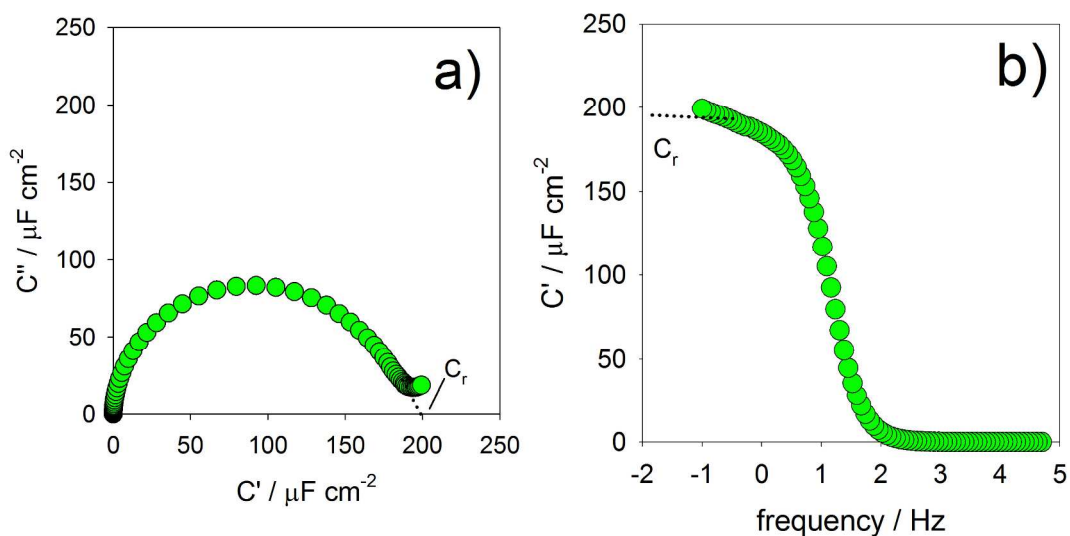


Figure 7. (a) A Nyquist capacitive plot of a 6-ferrocenyl-hexanethiol film in 100 mM TBA PF₆ dichloromethane as obtained by CS. Note that impedance spectra (obtained through normal electrochemical impedance spectroscopy) are converted into this analogous capacitance plots as detailed in the SI.^{2, 6} The SAM non-faradaic ionic relaxation contributes to less than 1% of the response at higher frequency and was subtracted following a procedure described in previous work (more details in SI. section 1.2).^{2, 3} (b) Bode capacitive plot of the real component of the complex capacitance function. Note that (a) and (b) correspond to the response associated with redox energy level occupancy at the half-wave potential (i.e. where the electrode Fermi level electrons equalise in energy to accessible orbital states of the redox layer). This density [$e^2(\delta N_R/\delta E)_v = e^2 g_r(E_F)$] corresponds to that of a single energy level, i.e. the half-wave electrode potential.

In summary, gold metallic states that are energetically aligned with oxidized iron states in the molecule contribute to a re-shaped molecular DOS and an enhanced charging efficiency (and thus enhanced C_r). Significantly, capacitive charging of the isolated molecule is both experimentally undetectable and energetically more demanding (see Table 1). In considering how sensitive the detectable capacitance is to orbital occupancy/electron density ($\delta\rho_R(N)/\delta\mu(N)$) changes it is instructive to note that this is expected to be greater the softer the system, as is the particular case of molecule-electrode system.¹

Finally, the experimentally resolved quantum capacitive term (proportional to the DOS) in CS experiments (Figure 7) can be theoretically rationalized and quantified by DFT. CS spectra obtained in Figure 7a and Figure 7b

¹ Note that we are herein considering the softness in terms of redox occupation instead of polarizability of the redox center or molecule itself, following the reasoning given by Eqn. (12).

correspond to measurements conducted at the electrochemical half wave potential where the capacitance is maximized^{2, 5, 6} (when the redox states responsible are equally populated). A quantitative comparison with experiment can be achieved by considering the particular situation when Eqn. (18) equates to Eqn. (14), resulting in $C_q = e^2 g_r(E) = e^2 (\delta N_R / \delta E)_v$. Since $C_q \sim C_r$, experimentally resolved C_r is highly dependent on the DOS situation theoretically predicted in Figure 6*b*. In moving DFT calculations to include a more experimentally realistic depiction of molecular films we use a cluster comprising 25 alkylferrocene molecules tethered to a metal slab (retaining the geometries previously identified). These calculations (detailed in the SI section 1.4) then report $C_q = e^2 g_r(E_F) \sim 230 \mu\text{F cm}^{-2}$, in good quantitative agreement with that resolved experimentally by CS for these films ($\sim 200 \mu\text{F cm}^{-2}$ – see Figure 7*a* and 7*b*).

4. CONCLUSIONS AND FINAL REMARKS

The computationally simple DFT calculations outlined herein overlay satisfyingly with electrochemical experimental observations (within CS experiments) since both are concerned with a consideration of parameters that are direct functions of the density of chargeable states. The density of the chargeable states was demonstrated herein to be that associated with frontier Kohn-Sham orbitals (the occupation of HOMO and LUMO frontier orbitals) with their respective eigenvalues. Since the redox characteristics of the surface bound molecules are, of course, implicitly governed by the surface potential tuned alignment between these and electrode states, it follows that redox capacitance is heavily influenced by the additional states introduced directly into HOMO-LUMO gap during surface assembly.

An important DFT-supported observation is that charging efficiency correlates strongly with chemical softness of the orbital states responsible. It was further resolved that interfacial charging is dominated by the oxidized ferrocene states because it is here where energetic alignment with metal states is optimal. The theoretical framework presented here, based on conceptual DFT analysis is, then, general at any level of modern electronic structure theory (ie beyond DFT definitions of electronic structure). The redox analysis it supports represents a general and valuable means of predicting experimental electrochemical observations and lays groundwork for

an optimized approach in generating molecular films of either very high charging capacity or highly environmentally responsive charging.

ACKNOWLEDGMENT

This work was supported by the São Paulo research Foundation (FAPESP, 2012-22820-7), Brazilian National Council for Scientific and Technological Development (CNPq) and UNESP grants.

REFERENCES

1. S. Luryi, *Applied Physics Letters* **52**, 501 (1988).
2. P. R. Bueno, G. Mizzon and J. J. Davis, *Journal of Physical Chemistry B* **116** (30), 8822-8829 (2012).
3. P. R. Bueno, F. Fabregat-Santiago and J. J. Davis, *Analytical Chemistry* **85** (1), 411-417 (2013).
4. B. E. Conway, *Electrochemical Supercapacitors: Scientific Fundamentals and Technological Applications*. (Springer, Berlin, 1999).
5. P. R. Bueno and J. J. Davis, *Analytical Chemistry* **86** (3), 1337-1341 (2014).
6. P. R. Bueno and J. J. Davis, *Anal. Chem.* **86** (4), 1977-2004 (2014).
7. M. Büttiker, H. Thomas and A. Prêtre, *Phys. Lett. A* **180**, 364-369 (1993).
8. F. C. B. Fernandes, M. S. Goes, J. J. Davis and P. R. Bueno, *Biosensors & Bioelectronics* **50**, 437-440 (2013).
9. F. C. B. Fernandes, A. Santos, D. C. Martins, M. S. Goes and P. R. Bueno, *Biosensors & Bioelectronics* **57**, 96-102 (2014).
10. J. Lehr, G. C. Hobhouse, F. C. B. Fernandes, P. R. Bueno and J. J. Davis, *Analytical Chemistry* **86** (7), 3682-3682 (2014).
11. P. Hohenberg and W. Kohn, *Physical Review B* **136** (3B), B864+ (1964).
12. F. De Proft and P. Geerlings, *Chemical Reviews* **101** (5), 1451-1464 (2001).
13. P. Senet, *Journal of Chemical Physics* **107** (7), 2516-2524 (1997).
14. H. Chermette, *Journal of Computational Chemistry* **20** (1), 129-154 (1999).
15. P. W. Ayers, J. S. M. Anderson and L. J. Bartolotti, *International Journal of Quantum Chemistry* **101** (5), 520-534 (2005).
16. R. G. Parr and W. T. Yang, *Annual Review of Physical Chemistry* **46**, 701-728 (1995).
17. P. Senet, *Journal of Chemical Physics* **105** (15), 6471-6489 (1996).
18. R. G. Parr and Y. Weitao, *Density-Functional Theory of Atoms and Molecules*. (Oxford Science Publication, 1994).
19. R. Car and M. Parrinello, *Physical Review Letters* **55** (22), 2471-2474 (1985).
20. A. J. Bard and L. R. Faulkner, *Electrochemical Methods Fundamentals and applications*, 2 ed. (John Wiley & Sons, 2000).
21. R. A. Marcus, *J. Phys. Chem.* **72** (3), 891-& (1968).
22. R. A. Marcus, *Angewandte Chem.* **32** (8), 1111-1121 (1993).
23. R. A. Marcus and N. Sutin, *Biochim. Biophys. Acta* **811** (3), 265-322 (1985).
24. G. J. Iafrate, K. Hess, J. B. Krieger and M. Macucci, *Physical Review B* **52** (15), 10737-10739 (1995).
25. J. Luo, Z. Q. Xue, W. M. Liu, J. L. Wu and Z. Q. Yang, *Journal of Physical Chemistry A* **110** (43), 12005-12009 (2006).
26. (Wikipedia, Finite difference method).
27. T. T. Heikkilä, *The Physics of Nanoelectronics*. (Oxford University Press, Oxford, 2013).
28. P. R. Bueno, T. A. Benites, M. S. Goes and J. J. Davis, *Analytical Chemistry* **85** (22), 10920-10926 (2013).

